Check for updates

# Terahertz time-domain spectroscopy as a novel tool for crystallographic analysis in cellulose: cellulose I to cellulose II, tracing the structural changes under chemical treatment

**Han Wang · Hiroki Kataoka · Satoru Tsuchikawa · Tetsuya Inagaki**

**Abstract** Terahertz time-domain spectroscopy (THz-TDS) has expanded possibilities in cellulose crystallography research, as THz radiation detects most intermolecular vibrations and responds to the phonons of crystalline lattices. In this study, we traced the transformation of the cellulose crystalline lattice from cellulose I to cellulose II by THz-TDS and X-ray powder diffraction. Cellulose II was obtained by treating cellulose I with NaOH of different concentrations (0 wt%–20 wt%, at 2 wt% intervals). The THz absorption coefficient spectra of cellulose II showed three characteristic peaks (at 1.32 THz, 1.76 THz, and 2.77 THz). The THz absorption coefficient spectra of cellulose II treated with 20-wt% NaOH and cellulose I without NaOH treatment were fitted by a seventh-order Fourier series. Thus, the THz absorption coefficient spectra of samples treated with NaOH of other concentrations could be considered a combination of these two fitted profiles of cellulose I and cellulose II, multiplied by different coefficients. Furthermore, the coefficients could reflect the relative contents of cellulose I and cellulose II in the samples.

H. Wang · H. Kataoka · S. Tsuchikawa · T. Inagaki (✉)
Graduate School of Bioagricultural Sciences, Nagoya University, Nagoya, Aichi 464-8601, Japan
e-mail: inatetsu@agr.nagoya-u.ac.jp

## Introduction

Cellulose II has a monoclinic crystalline sutrcture, containg two anti-parallel independent chains (Kolpak and Blackwell 1976; Langan et al. 1999), which can be obtained by mercerization (alkali treatment) or regeneration (recrystallization after solubilization) of native cellulose (Hermans and Weidinger 1946). After the alkali treatment such as NaOH of cellulose, both the crystalline lattice structure and the crystallinity change, therefore, tracing the transformation of the crystalline structure is essential for a better understanding of the processes of industry and biosynthesis where cellulose is involved, such as viscose rayon manufacturing (O'sullvian 1997; Brown 2004). Several techniques have been used to investigate the transformation of cellulose I to cellulose II, and X-ray diffraction (XRD) is the most widely applied technique (El-Oudiani et al. 2011; Kafle et al. 2014). Oh et al. observed that multiple bands of the Fourier-transform infrared (FTIR) spectra of cellulose I shift after NaOH treatment, and the absorbance ratios correlate with the crystallinity obtained from XRD patterns (Oh et al. 2005). Halonen et al. (2013) reported on the use of solid-state cross polarization/magic angle spinning carbon 13 nuclear magnetic resonance (CP/MAS 13C NMR) spectroscopy to investigate this

process, Raman spectroscopy and near-infrared (NIR) spectroscopy have also been used in such investigation (Schenzel and Fischer 2001; Schenzel et al. 2009).

Terahertz (THz) radiation lies in the frequency of 0.1–10 THz, which corresponds to the wavelengths of 3–0.03 mm (which lie at the interval between microwaves and infrared radiation). with characteristics of very low photon energy (1THz is about 4 meV), harmless to the human body and has better transmittance than infrared, visible light, etc,. Rapid progress has been made in THz technology in the past two decades, and one of the earliest commercial applications was THz time-domain spectroscopy (THz-TDS). Given that THz radiation detects the vibrations of many biomolecules and hydrogen bonds and directly responds to the phonons in crystal lattices, THz-TDS has been used in many fields which include investigation of the pharmaceutical polymorphs and the crystallinity (Strachan et al. 2005; Zeitler et al. 2007); quantitative characterization of paper and wood (Reid and Fedosejevs 2006; Todoruk et al. 2012; Inagaki et al. 2014; Peccianti et al. 2017; Wang et al. 2019); and detection of the vibrational modes of water isotopes (Fellers et al. 1999; Yada et al. 2009), DNA (Markelz et al. 2000; Markelz 2008; Arora et al. 2012), and protein (Ebbinghaus et al. 2007; Shiraga et al. 2016). Some case studies have confirmed the possibility of using THz-TDS for cellulose research, such as studies determining the crystallinity of cellulose I (Vieira and Pasquini 2014; Wang et al. 2021) and distinguishing cellulose I allomorphs (Wang et al. 2020).

As a follow-up to a previous study (Wang et al. 2020, 2021), the current work further explores the possibility of using THz-TDS in the research field of cellulose crystallography. It is the first study that traced the transformation of the crystalline lattice of cellulose I to that of cellulose II by using THz-TDS. The cellulose II sample was obtained by treating cellulose I with NaOH of different concentrations. Treatment of cellulose I with NaOH of concentrations exceeding 10% changed the crystalline lattice structure into that of cellulose II, as confirmed by other methods (such as XRD); the transformation was also reflected in the THz absorption coefficient spectra. The THz absorption coefficient spectra of cellulose I showed two absorption peaks; the absorption peak at 3.04 THz was shared by the allomorphs of $I_\alpha$ and

$I_\beta$, and the absorption peaks at 2.13 THz and 2.38 THz were characteristic absorption peaks of $I_\beta$ and $I_\alpha$, respectively (Wang et al. 2020, 2021). The THz absorption coefficient spectra of cellulose II showed a different profile of cellulose I, where the absorption peaks were at 1.32 THz, 1.76 THz, and 2.77 THz; the peak intensity of cellulose II was relatively small compared with that of cellulose I. The THz absorption coefficient spectra of cellulose II and cellulose I were fitted by a seventh-order Fourier series. The THz absorption coefficient spectra of the samples treated with NaOH of other concentrations could be considered a combination of the profiles of cellulose I and cellulose II; only the multiplied coefficients were different, and these coefficients could reflect the change in the relative content of the two components. Thus, the THz absorption coefficient spectra can be used to investigate the transformation of the crystalline lattice during the chemical treatment and the relative content of cellulose I and cellulose II of the mixed cellulose samples.

## Experimental

### Sample preparation

For observing the transformation from cellulose I to cellulose II, microcrystalline cellulose (MCC) powders (cellulose I, EMD Millipore 1.02331.0500) were treated with NaOH of different concentrations (0 wt%, 2 wt%, 4 wt%, 6 wt%, 8 wt%, 10 wt%, 12 wt%, 14 wt%, 16 wt%, 18 wt%, and 20 wt%) for 30 min at room temperature. After the reaction, the sample was washed with acetic acid and distilled water up to pH 7 and filtered. Then, the washed cellulose powders were dried in a desiccator containing $P_2O_5$. The NaOH, acetic acid, and phosphorus pentoxide used here were all purchased from KISHIDA CHEMICAL Co., Ltd. In this study, MCC samples without NaOH treatment were considered as cellulose I standard samples, while MCC samples treated with 20% NaOH were considered as standard cellulose II samples.

The above powders (treated with NaOH of different concentrations) were collected at a mass of 0.075 g by an electronic balance ($\pm 0.0001$ g). All the powders were compressed into tablets with a diameter of 14 mm and a thickness of approximately 0.35 mm using a compact heating press (IMC-180C,

Imoto Machinery Co., Ltd.). Three tablets were prepared for each powder to ensure reproducibility of the experiment. The thickness of these tablet samples was measured using a micrometer ($\pm 0.001$ mm).

### XRD and THz-TDS measurement

XRD measurement of all the tablet samples was performed with Cu-K$\alpha$ radiation ($\lambda = 0.1542$ nm) using an X-ray diffractometer (Ultima IV, Rigaku) at a voltage of 40 kV and a current of 40 mA. Diffractograms were recorded from 5° to 40°. The scan speed was set to 5° min$^{-1}$, and the sampling step was 0.05°. The background diffractogram was obtained from an empty sample holder.

The THz transmission spectra of all the tablet samples were measured by using a Tera Prospector (Nippo Precision Co., Ltd.), and the reference signals were obtained by measurement of air before and after sample measurement. The THz beam was horizontally polarized with a bandwidth of about 0.1 THz to 4.00 THz, and the spectral resolution was 0.02 THz, which corresponded to the inverse of the temporal scan range (50 ps). The diameter of the THz beam spot on the sample was around 3 mm. Each measurement was recorded by averaging 100 scans to improve the signal-to-noise ratio. For reproducibility, all measurements were conducted thrice. To avoid the influence of the THz absorption of water vapor on the measurement, we placed the whole THz optical system in an almost-closed acrylic box, which was filled with dry air until all the THz measurements were completed to ensure stability of humidity. All samples were placed in the box for 24 h before measurement to balance the ambient humidity.

### Results and discussion

#### XRD pattern and THz absorption spectrum analysis of cellulose treated with NaOH

The original XRD pattern was cut out with a scattering range of 10° to 30° and processed with background subtraction and baseline correction as arranged in Fig. 1 with the color gradient expressing the different concentrations of NaOH during the treatment. The three main crystalline peaks of cellulose I had Miller indices of ($1\bar{1}0$), (110), and (200);
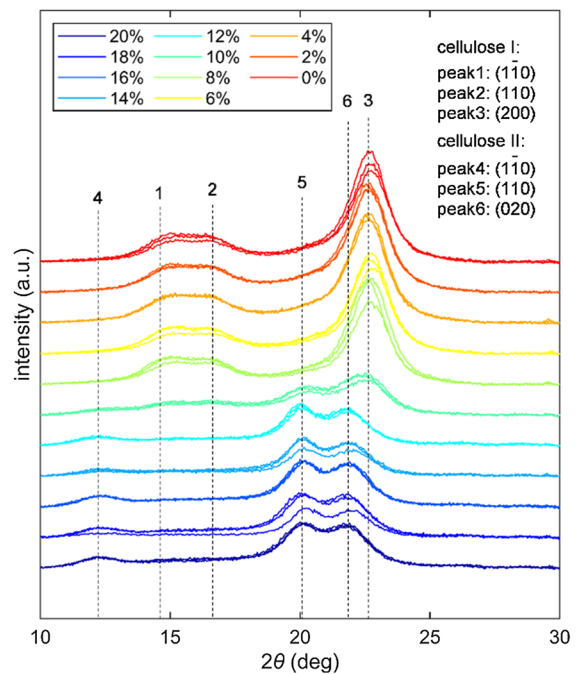


**Fig. 1** Baseline-corrected XRD patterns of all cellulose samples (the gradient colors express the different concentrations of NaOH during the treatment), the crystalline peaks of cellulose I and II are denoted as numbers

for cellulose II, the Miller indices were ($1\bar{1}0$), (110), and (020). In Fig. 1, the crystalline peaks of cellulose I are denoted as peak1, peak2, and peak3, and those of cellulose II are denoted as peak4, peak5, and peak6. The changes in the XRD patterns after the NaOH treatment can be easily identified; under treatment with 0% to 8% NaOH, typical cellulose I patterns can be observed. With the increase in NaOH concentration, the pattern treated with 10% NaOH showed a superimposition of the cellulose I and cellulose II patterns, and the samples treated with 12% to 20% NaOH showed patterns dominated by the cellulose II pattern.

In order to obtain the crystalline index of cellulose I and II which will be discussed in the next section, the six crystalline peaks as described above, and two amorphous intensity curves for cellulose I and II, respectively, were deconvoluted via a curve-fitting process using a pseudo-Voigt profile, which has been used in many other research cases. Considering that this method is widely used, the detailed process of this part will not be repeated here. The

background subtraction, baseline correction and deconvolution process of the XRD pattern are all provided in the Supplementary Information.

The measured THz time-domain signal was Fourier transformed into the frequency domain, and the absorption coefficient $\alpha$ was calculated using the following equations:

$$n = -\frac{\varphi c}{2\pi v L} + 1 \tag{1}$$

$$\alpha = -\frac{2}{L} \ln\left[R\frac{(n+1)^2}{4n}\right] \tag{2}$$

where $\varphi$ is the phase difference between the reference and measured samples ($\varphi_{reference} - \varphi_{sample}$), $R$ is the ratio of the amplitude in the frequency domain of the measured samples to the reference, $c$ is the speed of light ($3 \times 10^8$ m/s), $v$ is the frequency, and $L$ is the thickness of the samples (Reid and Fedosejevs 2006).

The original THz absorption coefficient spectra from 0.2 THz to 3.5 THz were shown in Fig. 2a, and corrected for baseline fluctuations with a standard normal variate (SNV) algorithm and then smoothed by the application of a Savitzky–Golay filter with a second-order polynomial and 21 smoothing points to remove the noise, as shown in Fig. 2b, wave numbers are also given here for comparison with the classical vibrational spectroscopy, the used color gradient is the same as that in Fig. 1. The THz absorption coefficient spectra of all the cellulose samples (including those treated with/without NaOH) showed a similar change trend as that of the XRD patterns. The absorption characteristics are shown in the THz absorption coefficient spectra of cellulose I and cellulose II totally differed from those of other spectroscopy, such as FTIR spectra (which show a peak shift after NaOH treatment of cellulose (Oh et al. 2005)). At NaOH concentrations below 10%, the THz absorption coefficient spectra showed the typical characteristics of cellulose I observed in previous studies: the absorption peak at 2.13 THz corresponded to the cellulose $I_\beta$ type (Wang et al. 2020), and the absorption peak at 3.04 THz correlated with the amount of cellulose I, regardless of the $I_\alpha$ and $I_\beta$ allomorphs (Wang et al. 2021). The integrated intensity of this absorption coefficient peak (3.04 THz) in can be used to evaluate the crystallinity of cellulose $I_\beta$ (Wang et al. 2021). For the 20% NaOH–treated cellulose samples, which
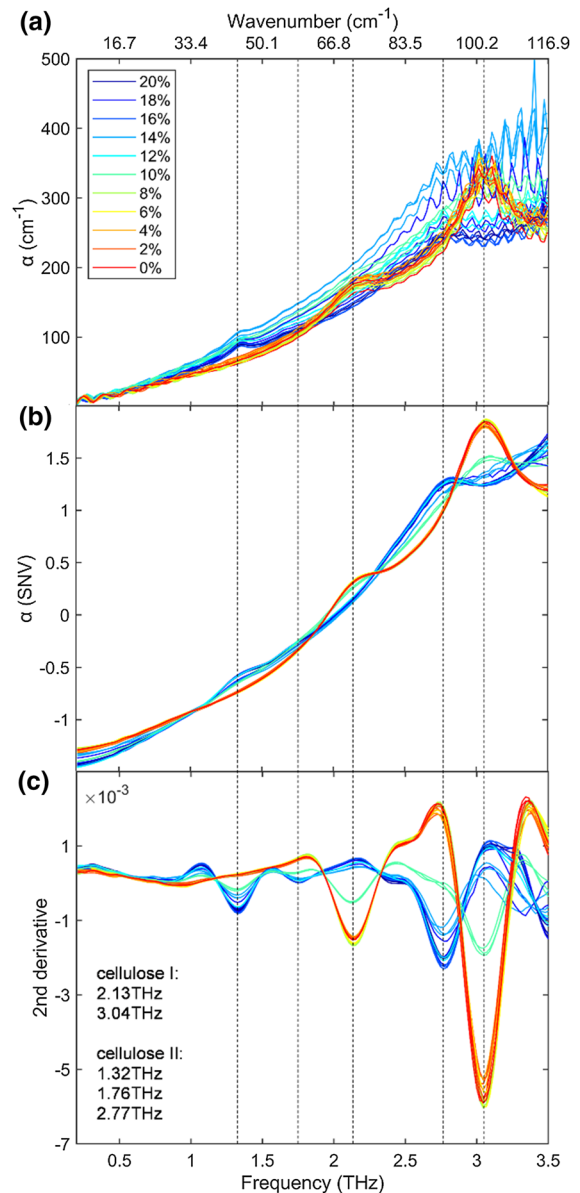


**Fig. 2** THz spectra of cellulose treated with NaOH of different concentrations. **a** The original THz absorption coefficient spectra, **b** SNV and smoothed THz absorption coefficient spectra, **c** second derivative of the THz absorption coefficient spectra

were almost cellulose II, the absorption coefficient spectra showed different characteristics of cellulose I; two absorption peaks (at 1.32 THz and 2.77 THz) can be directly observed. Given that the absorption peaks in the THz region of cellulose II were smaller than those of cellulose I, the Savitzky–Golay second derivative of the THz absorption coefficient spectra was

examined to distinguish the absorption peaks clearly as shown in Fig. 2c. The peaks at 1.32 THz, 1.76 THz, and 2.77 THz could be easily observed, whereas the peak at 1.76 THz was almost invisible in the
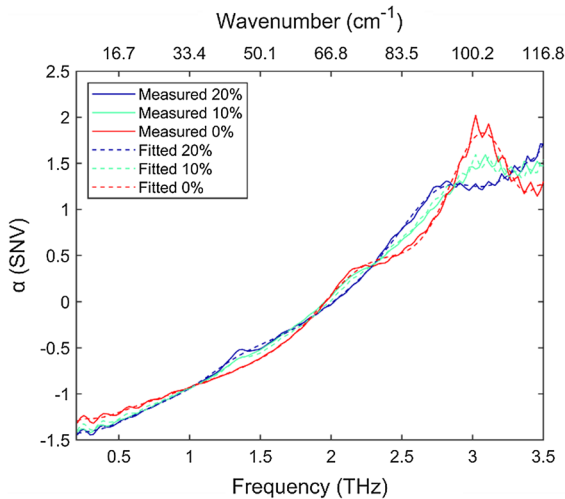


**Fig. 3** THz absorption coefficient spectra of cellulose treated with 20% (blue), 10% (green), and 0% (red) NaOH that are measured (after SNV) and curve fitted using a 7th Fourier series

THz absorption coefficient spectra. The THz absorption coefficient spectra of cellulose treated with 10% NaOH showed the characteristics of both cellulose I and cellulose II as that in the XRD patterns (Fig. 3).

The peak positions of the THz absorption coefficient spectra, $2\theta$ values, and d-spacing values calculated from the XRD patterns of different types of cellulose are summarized in Table 1. The d-spacing values were calculated as follows:

$$d = \frac{\lambda}{2\sin\theta} \tag{3}$$

where $\lambda$ is the wavelength of the X-ray radiation (0.1542 nm) and $\theta$ is the Bragg angle (Bragg and Bragg 1913). As shown in Table 1, the change in the crystalline structures was reflected in the observed d-spacing values, the $2\theta$ of the XRD patterns, and the peak positions of the THz absorption coefficient spectra. Generally speaking, the higher the frequency, the greater the photon energy. Cellulose I—whether $I_\beta$ or $I_\alpha$—showed a common absorption peak at 3.04 THz. The THz absorption peak at 2.13 THz of cellulose $I_\beta$ was located at a lower frequency compared with that of cellulose $I_\alpha$ at 2.38 THz, which may be caused by the more stable crystalline structure of

**Table 1** $2\theta$ and d-spacing values calculated from the XRD patterns and the peak positions of THz absorption coefficient spectra

| | XRD pattern | | | | | | THz absorption spectrum | | |
|---|---|---|---|---|---|---|---|---|---|
| | $2\theta$ (°) | | | d-spacing (nm) | | | Peak position (THz) | | |
| | $(1\bar{1}0)$ | (110) | (200)/(020)[*] | $(1\bar{1}0)$ | (110) | (200)/(020)[*] | peak1 | peak2 | peak3 |
| Cellulose $I_\alpha$ (*Glaucocystis*)[a] | 14.71 | 17.04 | 22.89 | 0.602 | 0.520 | 0.389 | 2.38 | 3.04 | NaN |
| | 14.58 | 16.93 | 22.78 | 0.607 | 0.524 | 0.390 | 2.38 | 3.04 | NaN |
| | 14.57 | 16.91 | 22.77 | 0.608 | 0.524 | 0.391 | 2.38 | 3.04 | NaN |
| Cellulose $I_\beta$ (*Halocynthia*)[a] | 14.89 | 16.7 | 22.98 | 0.595 | 0.531 | 0.387 | 2.13 | 3.04 | NaN |
| | 14.94 | 16.75 | 23.04 | 0.593 | 0.529 | 0.386 | 2.13 | 3.04 | NaN |
| | 15.03 | 16.84 | 23.1 | 0.589 | 0.527 | 0.385 | 2.13 | 3.04 | NaN |
| Cellulose $I_\beta$ (without NaOH treated MCC) | 14.50 | 17.00 | 22.50 | 0.611 | 0.522 | 0.395 | 2.13 | 3.04 | NaN |
| | 14.54 | 16.81 | 22.50 | 0.610 | 0.522 | 0.395 | 2.13 | 3.04 | NaN |
| | 14.54 | 16.99 | 22.50 | 0.611 | 0.522 | 0.395 | 2.13 | 3.04 | NaN |
| Cellulose II (20% NaOH treated MCC) | 12.50 | 20.24 | 22.00 | 0.709 | 0.434 | 0.404 | 1.32 | 1.76 | 2.77 |
| | 12.50 | 20.45 | 21.09 | 0.708 | 0.440 | 0.404 | 1.32 | 1.76 | 2.77 |
| | 12.50 | 20.50 | 22.00 | 0.708 | 0.439 | 0.404 | 1.32 | 1.76 | 2.77 |

*The Miller indices for cellulose I and cellulose II were (200) and (020), respectively

[a]The values were adopted from Wang et al. (2020)

cellulose $I_\beta$ than that of cellulose $I_\alpha$. The THz absorption peaks of cellulose II were distributed at a lower frequency, which may be related to the more stable and lower overall energy of cellulose II (Langan et al. 1999, 2001). As shown in Table 1, the $2\theta$ of the same cellulose was inconsistent in XRD patterns, on the other hand, the position of the absorption peak of the THz absorption coefficient spectrum is very definite, only varying due to the crystalline form of cellulose. However, the specific assignments of these absorption peaks at the molecular level still need further research.

Crystallinity and relative content of cellulose (determined by XRD and THz)

The crystallinity index (CrI) calculated from the XRD patterns was determined by the following equation:

$$CrI = \frac{S_{Cr}}{S_{Cr} + S_{Am}} \tag{4}$$

where $S_{Cr}$ and $S_{Am}$ are the sums of the integrated intensity of six crystalline peaks and the amorphous

intensity curves, respectively. The detailed process of the peak deconvolution with the pseudo-Voigt profile is given in the Supplementary Information.

CrI was divided into CrI1 (for cellulose I) and CrI2 (for cellulose II), which were calculated as follows:

$$CrI1 = \frac{S_{Cr1}}{S_{Cr1} + S_{Cr2}} \cdot CrI \tag{5}$$

$$CrI2 = \frac{S_{Cr2}}{S_{Cr1} + S_{Cr2}} \cdot CrI \tag{6}$$

where $S_{Cr1}$ and $S_{Cr2}$ are the sums of the integrated intensity of the crystalline peaks of cellulose I and cellulose II, respectively, and $CrI$ is the crystallinity index calculated by Eq. (4).

CrI1 and CrI2 can be used to evaluate the relative content of cellulose I and cellulose II in the samples to grasp the progress of the NaOH treatment. The correlations of the concentrations of NaOH with CrI1 and CrI2 are shown in Fig. 4a, b, respectively. CrI1 and CrI2 showed completely opposite trends with the change in the NaOH concentration, where CrI1 decreased with the increase in the NaOH
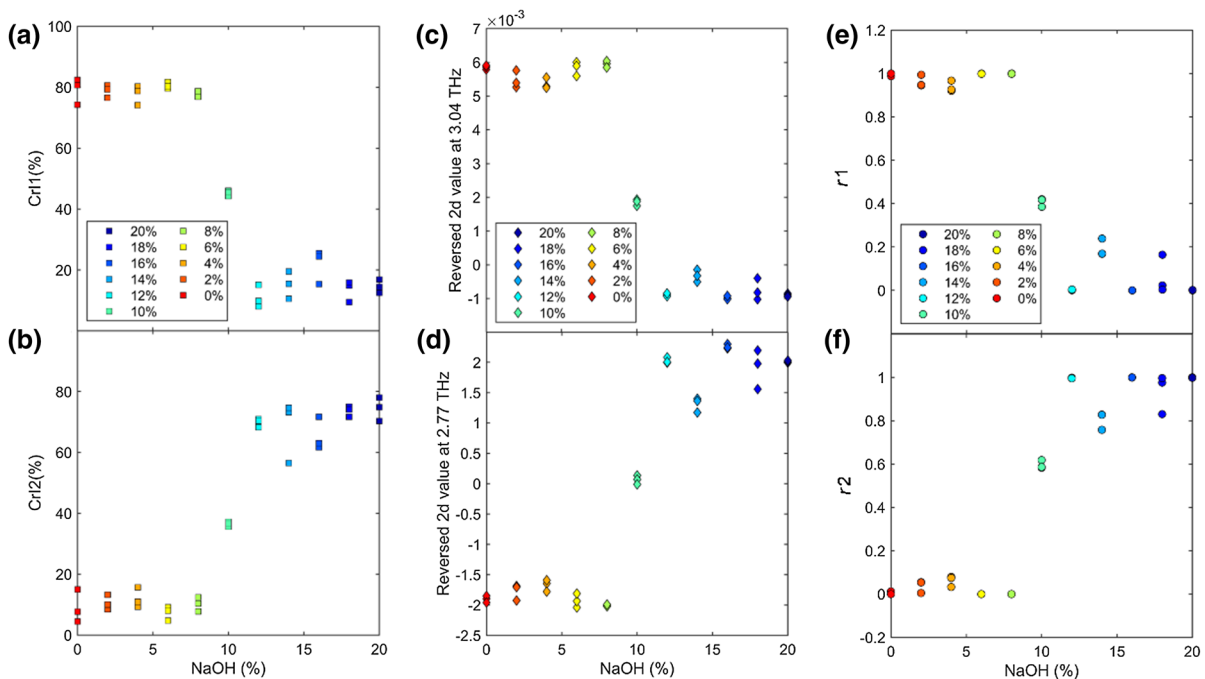


**Fig. 4** Correlation of the concentrations of NaOH with **a** CrI1 and **b** CrI2 calculated from the XRD patterns, reversed second derivative at **c** 3.04 THz and **d** 2.77 THz, and coefficients **e** $r1$ and **f** $r2$ fitted from the THz absorption coefficient spectra

concentration, indicating a decrease in the cellulose I in the samples. In contrast, CrI2 increased with the NaOH concentration, which showed a transformation from cellulose I to cellulose II. Both Fig. 4a, b showed inflection points at the 10% NaOH concentration, which indicated that the crystalline lattice transformed from cellulose I to cellulose II, as shown by the XRD patterns in Fig. 1.

As shown in Fig. 2, the THz absorption coefficient spectra of the 10% NaOH–treated sample also showed mixed characteristics of cellulose I and cellulose II, the other samples showed a characteristic of cellulose I (treated with NaOH < 10%) and cellulose II (treated with NaOH > 10%), respectively. The changes of the intensity are more easily observed in the second derivative of the THz absorption coefficient spectra, where the troughs correspond to the absorption peaks in the THz absorption coefficient spectra, and the reversed second derivative value reflects the intensity changes of the absorption peaks directly. As shown in Fig. 4c, d, the reversed second derivative values at 3.04 THz and 2.77 THz showed a similar trend of change of CrI1 and CrI2 calculated from XRD patterns.

Given the simplicity of the THz absorption coefficient and the above identification of the absorption peaks of cellulose I and cellulose II, the THz absorption coefficient spectra of the cellulose I without NaOH treatment and the cellulose II with 20% NaOH treatment can be written as two seventh-order Fourier series (denoted as $f(0)$ and $f(20)$). Furthermore, the expression of the THz absorption coefficient spectra of the samples treated with NaOH of other concentrations can be written as $f = r1 \cdot f(0) + r2 \cdot f(20)$, where $r1$ and $r2$ are coefficients determined by the curve-fitting process, and $r1 + r2 = 1$, since the samples only have two types of cellulose crystalline. As shown in Fig. 3, the fitted results reproduced the measured THz absorption coefficient spectra (only after SNV to correct the baseline fluctuations) to a certain degree. The specific parameters of the fitted Fourier series ($f(0)$ and $f(20)$) and the residual distribution are provided in Supplementary Information. The residuals follow a normal distribution, indicating the applicability of the fitting model.

The correlations of the NaOH concentrations with the coefficients $r1$ and $r2$ are shown in Fig. 4e, f. These correlations were highly similar with those of CrI1, CrI2 and reversed second derivative values

of THz absorption coefficient spectra. This indicated that the coefficients obtained from the fitting of the THz absorption coefficient can be used to evaluate the relative content of cellulose I and cellulose II. Furthermore, for the samples which only have two types of cellulose crystalline components, the coefficients $r1$ and $r2$ still may give a more accurate relative content of each crystalline component, since the integrated intensity of the THz mass absorption coefficient peak was very possible to directly reflect the amount of the cellulose crystalline without the interference of the amorphous region on the THz absorption coefficient spectra (Wang et al. 2021).

## Conclusions

In this study, cellulose I was treated with NaOH of different concentrations (from 0 to 20%) to change the crystalline structure. XRD patterns and THz absorption coefficient spectra of samples were obtained. The XRD patterns and the THz absorption coefficient spectra can be divided into three types; when the concentration of NaOH during processing was lower than 10%, equal to 10%, and higher than 10%, the XRD patterns and the THz absorption coefficient spectra showed a typical profile of cellulose I, mixed characteristics of cellulose I and cellulose II, and a typical profile of cellulose II, respectively. For the THz absorption coefficient spectra of cellulose I, only two absorption peaks (at 2.13 THz and 3.04 THz) could be observed. By contrast, three absorption peaks (at 1.32 THz, 1.76 THz, and 2.77 THz) could be observed for cellulose II. The XRD patterns were deconvoluted by using a pseudo-Voigt profile, and the calculated crystalline index can be further divided into CrI1 and CrI2 to indicate the relative content of cellulose I and cellulose II in the samples, respectively. CrI1 decreased as the concentration of NaOH increased, whereas CrI2 increased with the NaOH concentration. The THz absorption coefficient spectra of cellulose I without NaOH treatment and cellulose II treated with 20% NaOH were fitted by the seventh-order Fourier series ($f(0)$ and $f(20)$). After this process, all the THz absorption coefficient spectra could be fitted as a mixture of these two formulae by multiplying two coefficients ($r1$ and $r2$), which meant that $f = r1 \cdot f(0) + r2 \cdot f(20)$. The correlations between the concentrations of NaOH and $r1$ and $r2$ showed

similar changing trends of CrI1 and CrI2. Remarkably, the transformation of the crystalline lattice from cellulose I to cellulose II after the NaOH treatment can be traced by THz absorption coefficient spectra the coefficients $r1$ and $r2$ are able to describe the relative content of cellulose I and cellulose II in a sample. The THz signal can be measured at room temperature and does not require sample pretreatment, the measurement and analysis processes are rapid and simple compared with the XRD patterns. Combined with the results of previous research, we believe THz-TDS has the potential to become a useful tool in the research and understanding of cellulose crystallography.

**Author contribution** Han Wang and Tetsuya Inagaki conceived and designed the experiments. Han Wang and Hiroki Kataoka performed the experiments and analyzed the data. Han Wang wrote the paper, Tetsuya Inagaki and Satoru Tsuchikawa gave final approval of the manuscript.

**Code availability** Matlab 2018b.

**Declarations**

**Conflict of interest** The author declare that they have no conflict of interest.

**Ethical standards** This study following Compliance with Ethical Standards; this study does not involve human participants, animals, and potential conflicts of interest.

# References

Arora A, Luong TQ, Krüger M et al (2012) Terahertz-time domain spectroscopy for the detection of PCR amplified DNA in aqueous solution. Analyst 137:575–579

Bragg WH, Bragg WL (1913) The reflection of X-rays by crystals. Proc R Soc London Ser A Contain Pap Math Phys Character 88:428–438

Brown RM (2004) Cellulose structure and biosynthesis: what is in store for the 21st century? J Polym Sci A Polym Chem 42:487–495

Ebbinghaus S, Seung JK, Heyden M et al (2007) An extended dynamical hydration shell around proteins. Proc Natl Acad Sci USA 104:20749–20752

El-Oudiani A, Chaabouni Y, Msahli S, Sakli F (2011) Crystal transition from cellulose i to cellulose II in NaOH treated *Agave americana* L. fibre. Carbohydr Polym 86:1221–1229

Fellers RS, Leforestier C, Braly LB et al (1999) Spectroscopic determination of the water pair potential. Science 284:945–948

Halonen H, Larsson PT, Iversen T (2013) Mercerized cellulose biocomposites: a study of influence of mercerization on cellulose supramolecular structure, water retention value and tensile properties. Cellulose 20:57–65

Hermans PH, Weidinger A (1946) On the recrystallization of amorphous cellulose. J Am Chem Soc 68:2547–2552

Inagaki T, Ahmed B, Hartley ID et al (2014) Simultaneous prediction of density and moisture content of wood by terahertz time domain spectroscopy. J Infrared Millimeter Terahertz Waves 35:949–961

Kafle K, Greeson K, Lee C, Kim SH (2014) Cellulose polymorphs and physical properties of cotton fabrics processed with commercial textile mills for mercerization and liquid ammonia treatments. Text Res J 84:1692–1699

Kolpak FJ, Blackwell J (1976) Determination of the structure of cellulose II. Macromolecules 9:273–278

Langan P, Nishiyama Y, Chanzy H (1999) A revised structure and hydrogen-bonding system in cellulose II from a neutron fiber diffraction analysis. J Am Chem Soc 121:9940–9946

Langan P, Nishiyama Y, Chanzy H (2001) X-ray structure of mercerized cellulose II at 1 Å resolution. Biomacromol 2:410–416

Markelz AG (2008) Terahertz dielectric sensitivity to biomolecular structure and function. IEEE J Sel Top Quantum Electron 14:180–190

Markelz AG, Roitberg A, Heilweil EJ (2000) Pulsed terahertz spectroscopy of DNA, bovine serum albumin and collagen between 0.1 and 2.0 THz. Chem Phys Lett 320:42–48

O'sullvian AC (1997) Cellulose: the structure slowly unravels. Cellulose 4:173–207

Oh SY, Dong IY, Shin Y et al (2005) Crystalline structure analysis of cellulose treated with sodium hydroxide and carbon dioxide by means of X-ray diffraction and FTIR spectroscopy. Carbohydr Res 340:2376–2391

Peccianti M, Fastampa R, Mosca Conte A et al (2017) Terahertz absorption by cellulose: application to ancient paper artifacts. Phys Rev Appl 7:064019

Reid M, Fedosejevs R (2006) Terahertz birefringence and attenuation properties of wood and paper. Appl Opt 45:2766–2772

Schenzel K, Fischer S (2001) NIR FT Raman spectroscopy: a rapid analytical tool for detecting the transformation of cellulose polymorphs. Cellulose 8:49–57

Schenzel K, Almlöf H, Germgård U (2009) Quantitative analysis of the transformation process of cellulose I → cellulose II using NIR FT Raman spectroscopy and chemometric methods. Cellulose 16:407–415

Shiraga K, Ogawa Y, Kondo N (2016) Hydrogen bond network of water around protein investigated with terahertz and infrared spectroscopy. Biophys J 111:2629–2641

Strachan CJ, Taday PF, Newnham DA et al (2005) Using terahertz pulsed spectroscopy to quantify pharmaceutical polymorphism and crystallinity. J Pharm Sci 94:837–846

Todoruk TM, Hartley ID, Reid ME (2012) Origin of birefringence in wood at terahertz frequencies. IEEE Trans Terahertz Sci Technol 2:123–130

Vieira FS, Pasquini C (2014) Determination of cellulose crystallinity by terahertz-time domain spectroscopy. Anal Chem 86:3780–3786

Wang H, Inagaki T, Hartley ID et al (2019) Determination of dielectric function of water in THz region in wood cell wall result in an accurate prediction of moisture content. J Infrared Millimeter Terahertz Waves 40:673–687

Wang H, Horikawa Y, Tsuchikawa S, Inagaki T (2020) Terahertz time-domain spectroscopy as a novel tool for crystallographic analysis in cellulose. Cellulose 27:9767–9777

Wang H, Tsuchikawa S, Inagaki T (2021) Terahertz time-domain spectroscopy as a novel tool for crystallographic analysis in cellulose: the potentiality of being a new standard for evaluating crystallinity. Cellulose 28:5293–5304

Yada H, Nagai M, Tanaka K (2009) The intermolecular stretching vibration mode in water isotopes investigated with broadband terahertz time-domain spectroscopy. Chem Phys Lett 473:279–283

Zeitler JA, Kogermann K, Rantanen J et al (2007) Drug hydrate systems and dehydration processes studied by terahertz pulsed spectroscopy. Int J Pharm 334:78–84